Real-time Computation of Optimized Pulse Patterns for Compensation of Estimated Grid Voltage Harmonics

Ellis Tsekouras
School of Elec. and Data Eng.
University of Technology Sydney
Sydney, Australia
ellis.tsekouras@uts.edu.au

Ricardo P. Aguilera
School of Elec. and Data Eng.
University of Technology Sydney
Sydney, Australia
raguilera@ieee.org

Tobias Geyer
Motion System Drives
ABB Switzerland Ltd
Turgi, Switzerland
t.geyer@ieee.org

***Abstract*—For high-power converters, optimized pulse patterns (OPPs) offer unparalleled harmonic performance at low switching frequencies; making them a promising choice for grid-connected converters. However, in the presence of a distorted grid voltage, their harmonic performance deteriorates and pronounced harmonic currents can emerge. Consequently, their optimal harmonic performance cannot be ensured in practice since the grid voltage is typically not ideal. To address this challenge, a two-fold approach is proposed in this paper. Firstly, a Steady-State Kalman Filter (SSKF) is designed to estimate the grid voltage harmonics in real-time. Secondly, a new objective function that explicitly incorporates grid voltage harmonics in conjunction with grid code harmonic limits is given. From this, an OPP is computed in real-time to compensate for the effect of grid voltage harmonics without a lookup table (LUT) or complex data structure. To promote the proposal's technical feasibility, a detailed implementation of a real-time OPP solver on commercial hardware is given. Experimental results verify the improved harmonic performance of OPPs that incorporate distortions at a converter's point of common coupling (PCC) to the grid.**

***Index Terms*—Optimized Pulse Patterns (OPPs), grid-connected converters, Steady-State Kalman Filter (SSKF), distorted grid voltage, real-time OPPs**

I. Introduction

Selective Harmonic Elimination (SHE) and Selective Harmonic Mitigation (SHM) are popular modulation strategies that have a long history of being used for high-power converters [1]–[4]. Since then, optimized pulse patterns (OPPs) have emerged as the leading modulation strategy in terms of harmonic performance for switching frequencies below 1kHz [5] - as evidenced by ABB's successful commercialization of the ACS6080 industrial medium voltage (MV) AC motor drive. Recently, there is growing interest to commutate grid-connected converters with OPPs, such as inverters and STATCOMs [6]–[8], as opposed to SHE or SHM methods.

In practice, the grid voltage is not ideal. It is distorted with harmonics that arise from nonlinear loads and other converters [9]. This notion of a distorted grid voltage is supported by the Long Term National Power Quality Survey (LTNPQS) [10], [11]. For almost a decade, this project has been monitoring over 12,000 sites in Australia's electrical network that range from 230V - 132kV. A key finding from their harmonic spectrum data is the widespread prevalence of non-triplen odd (NTO) harmonics within the grid voltage [12]. For a converter, these grid voltage distortions can corrupt the current they inject at their PCC, thereby increasing THD and reducing efficiency.

The presence of grid voltage harmonics is a concern for OPPs[1] because they are formulated assuming an ideal grid voltage [13]–[15]. Consequently, by today's methods, this common assumption can jeopardize an OPP's optimal harmonic performance by introducing a susceptibility to grid voltage harmonics. Pre-computing OPPs and storing them in a LUT is not feasible either, as the magnitude and phase of distortions in the grid are generally unknown [16].

For AC motor drives, exploring OPPs for pre-determined non-sinusodial back-EMFs has been studied in [17]–[19]. Whereas for grid-connected applications, compensating OPPs for grid voltage harmonics is yet to be explored. A novel approach for SHE uses an Artificial Neural Network (ANN) to eliminate the lower-order harmonics for an Active Power Filter (APF) [20]. Despite showing promise at compensating pulse patterns that are formulated from $\leq$5 harmonics, this data structure approach may encounter a limitation if extended to pulse patterns that are formulated from a broader spectrum of harmonics - such as an OPP.

In contrast to relying on Look-up Tables (LUT) or complex data structures, this paper proposes to compensate OPPs for the effect of grid voltage harmonics in real-time. By acknowledging that harmonic performance, such as THD, is assessed in the steady-state and assuming that distortions in the grid change slowly with respect to their fundamental frequency, this may afford sufficient time to compute an OPP online.

The first challenge is estimating grid voltage harmonics in real-time. Fast Fourier Transformation (FFT) methods can be used to estimate harmonics. However, their computational burden, memory requirements and delay are a drawback. On the contrary, cascaded resonators or notch filters tuned to each

[1]It is equally concerning for SHE and SHM, since they too neglect grid voltage harmonics within their objective functions. Nonetheless, the focus of this work is on OPPs since they yield optimal harmonic performance.

harmonic are also capable [21]. A more promising alternative are Kalman Filters [22], [23]. In particular, the Steady-State Kalman Filter (SSKF) [24]–[26], as it is optimal and simple to implement. Secondly, a new objective function to compensate OPPs for these voltage harmonics must be minimized in real-time. Thirdly, an algorithm to interface this real-time OPP solver with an SSKF on commercial hardware is then needed.

Overcoming these three challenges is precisely how this paper is presented. In Section II, a SSKF is designed to estimate low-order harmonics in the grid-voltage. A distinctive feature of our proposal is the residual harmonics concept. It ensures unmodeled higher-order harmonics do not affect the SSKF's performance. Then, in Section III, a new objective function to compensate OPPs for these estimated voltage harmonics is given. Following this, a real-time OPP solving algorithm that consolidates and implements both proposals on commercial hardware is presented in Section IV. The experimental results of Section V then showcase the promising harmonic performance of grid-voltage-compensated OPPs under real-world conditions; a distorted grid voltage. A block diagram depicting this proposal is shown in Fig 1.

Throughout this paper, we assume the converter's PCC is an infinite bus that has balanced distortions of NTO harmonics. This assumption allows the converter to be neglected as a grid disturbance and a single OPP can be computed for all three phases. Weak and unbalanced grids are encountered in practice, such as off-shore wind farms or micro-grids. Therefore, exploring the estimation of voltage harmonics for weak and unbalanced grids in the context of OPPs is an important endeavor that is deserving of future work.

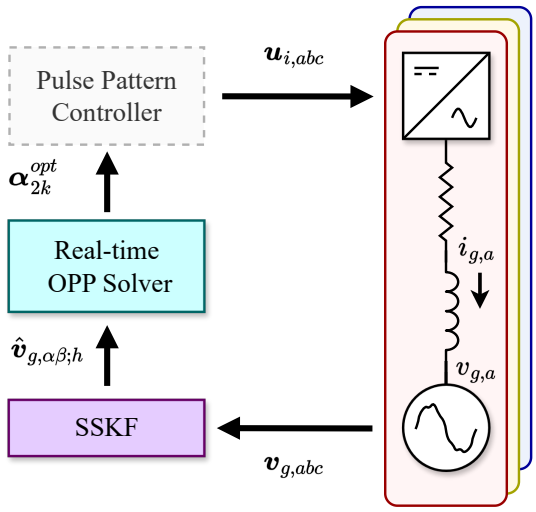

Fig. 1: Proposed block diagram for real-time computation of OPPs for compensation of estimated grid voltage harmonics. Interfacing the novel real-time OPPs with a Pulse Pattern Controller [28]–[30] is reserved for a sequel.

II. Optimal Estimation of Harmonics in Real-time

A. Quadrature Oscillator Model in Discrete-time

To yield a dynamic model for the n^{th} harmonic, a discrete-time quadrature oscillator model from [27] in $\alpha\beta$ is:

$$\boldsymbol{x}_n(k+1) = \boldsymbol{A}_n \cdot \boldsymbol{x}_n(k) \tag{1}$$

where $\boldsymbol{x}_n = [v_{g,\alpha;n}, v_{g,\beta;n}]^T$, $n \in \{1, -5, +7, ..., N\}$ considers only NTO harmonics of positive- and negative-sequence, and the state matrix is:

$$\boldsymbol{A}_n = \begin{bmatrix} \cos(n\omega_1 t_s) & -\sin(n\omega_1 t_s) \\ \sin(n\omega_1 t_s) & \cos(n\omega_1 t_s) \end{bmatrix} \tag{2}$$

Where ω_1 is the fundamental frequency and t_s is a fixed sampling time. By modeling each voltage harmonic as a cosine and sine wave, they are in quadrature and their phase can be computed as $\theta_n = \tan^{-1}(v_{g,\beta;n}/v_{\alpha;n})$. This is important for Section III, as a Park Transform will be applied to yield the Fourier Coefficients of each grid voltage harmonic.

B. Residual Harmonics

Estimating harmonics with Kalman Filters is not new [22]–[26]. However, one limitation in common with these existing methods is the need to estimate many harmonic components to improve their estimation performance. This occurs since the decoupled representation of a signal as integer harmonics is truncated and incomplete if an insufficient number of harmonics are modelled.

A novelty of the proposed approach is the introduction of a high process covariance state, denoted as the residual harmonics, h_{res}. This state is essentially a frequency bin that accumulates unmodelled harmonics. As a result, in contrast to what a Fourier Series stipulates, a Kalman Filter can then completely reconstruct an estimate of a signal from an arbitrary and finite number of harmonics.

C. System Model

By extrapolating (1), the system model for estimating up to the N^{th} NTO grid voltage harmonic is:

$$\boldsymbol{x}(k+1) = \boldsymbol{A} \cdot \boldsymbol{x}(k) \tag{3}$$

where,

$$\boldsymbol{A} = \begin{bmatrix} \boldsymbol{A}_1 & \boldsymbol{0} & \cdots & \boldsymbol{0} & \boldsymbol{0} \\ \boldsymbol{0} & \boldsymbol{A}_5 & \cdots & \boldsymbol{0} & \boldsymbol{0} \\ \vdots & \vdots & \ddots & \vdots & \vdots \\ \boldsymbol{0} & \boldsymbol{0} & \cdots & \boldsymbol{A}_N & \boldsymbol{0} \\ \boldsymbol{0} & \boldsymbol{0} & \cdots & \boldsymbol{0} & \boldsymbol{A}_{h_{res}} \end{bmatrix} \tag{4}$$

Note the residual harmonics state, h_{res}, is appended after the last modelled NTO harmonic, N. The grid voltage, $\boldsymbol{v}_{\alpha\beta}$, can then be completely reconstructed by summating the modelled and residual harmonics from (3):

$$\boldsymbol{y}(k) = \boldsymbol{C} \cdot \boldsymbol{x}(k) \tag{5}$$

where $\boldsymbol{y} = [v_{g,\alpha}, v_{g,\beta}]^T$ and $\boldsymbol{C} = [\boldsymbol{I}, \boldsymbol{I}, \cdots, \boldsymbol{I}, \boldsymbol{I}]$. For notational brevity, $\boldsymbol{0} = \boldsymbol{0}_{2\text{x}2}$, $\boldsymbol{I} = \boldsymbol{I}_{2\text{x}2}$ and k has been omitted when denoting elements in column vectors.

A linear time-invariant (LTI) system model of grid voltage harmonics in $\alpha\beta$ is now given by (3) and (5). This simple model can equally be applied to estimating current harmonics.

D. Steady-State Kalman Filter Design

The state estimation law for an LTI system with no input is:

$$\hat{\boldsymbol{x}}(k+1) = \boldsymbol{A}\hat{\boldsymbol{x}}(k) + \boldsymbol{L}(\boldsymbol{y}(k) - \boldsymbol{C}\hat{\boldsymbol{x}}(k)) \tag{6}$$

To determine the observer's gain, $\boldsymbol{L}$, the duality between control and estimation [31] can be applied to the Discrete-time Algebraic Ricatti Equation (DARE):

$$\boldsymbol{A}(\boldsymbol{P} - \boldsymbol{P}\boldsymbol{C}^T(\boldsymbol{R} + \boldsymbol{C}\boldsymbol{P}\boldsymbol{C}^T)^{-1}\boldsymbol{C}\boldsymbol{P})\boldsymbol{A}^T + \boldsymbol{Q} = \boldsymbol{P} \tag{7}$$

Where $\boldsymbol{Q}$ and $\boldsymbol{R}$ are the respective process and measurement covariance matrices that couple white gaussian noise into the system model. Solving (7) for $\boldsymbol{P}$, the optimal estimation gain for a linear quadratic estimator (LQE) is:

$$\boldsymbol{L} = \boldsymbol{A}\boldsymbol{P}\boldsymbol{C}^T(\boldsymbol{R} + \boldsymbol{C}\boldsymbol{P}\boldsymbol{C}^T)^{-1} \tag{8}$$

The estimation gain yielded from the recursive Kalman Filter algorithm invariably converges to (8) in the steady-state if the system is LTI [32], so an LQE and SSKF are equivalent.

To design an SSKF, $\boldsymbol{R}$ can be directly measured, since it encapsulates the covariance of the output sensors. Whereas for $\boldsymbol{Q}$, this is generally unknown as it encapsulates any parameter or modelling uncertainties, so designing it is an iterative process. Recalling that the intent of h_{res} is to yield a frequency bin state to accumulate the unmodelled harmonics, a comparably higher process covariance is assigned to it:

$$\boldsymbol{Q} = \rho_{obs} \cdot diag\,[\boldsymbol{I}, \boldsymbol{I}, \cdots, \boldsymbol{I}, 100 \cdot \boldsymbol{I},] \tag{9}$$

The scalar parameter ρ_{obs} can be adjusted to fine-tune the desired bandwidth and estimation performance.

E. Simulation Results

The rationale for proposing the residual harmonics concept is to improve the estimation performance of an SSKF - irrespective of how many harmonics are modelled. To explore the potential advantage of this proposal in the context of a distorted grid voltage, simulation results are shown in Fig. 2. The scenario is distorting the grid voltage with the 5^{th}-13^{th} NTO harmonics and comparing two SSKFs that are designed to estimate only the fundamental and 5^{th} harmonic.

The first SSKF, shown in Fig. 2a, is designed using a method similar to [25], [26]. Recalling (3), $\boldsymbol{A}$ then only includes $\boldsymbol{A}_1$ and $\boldsymbol{A}_5$. The second SSKF, shown in Fig. 2b, is designed using the proposed residual harmonics method, so an additional frequency bin state, $\boldsymbol{A}_{h_{res}}$, is appended to the system model.

Comparing the output estimation error, $\tilde{v}_{g,a}$, of Fig. 2a with the residual harmonic state of, $v_{g,\alpha;h_{res}}$, of Fig. 2b they are indistinguishable. This occurs since the residual harmonic state has successfully accumulated the unmodelled 7^{th}-13^{th} harmonics. In doing so, the output estimation error and overall performance of a SSKF for estimating harmonics in real-time is noticeably improved.

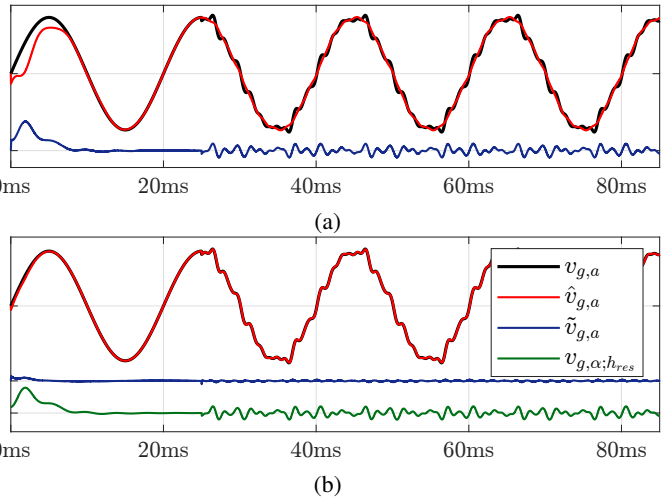

Fig. 2: Simulation results comparing the output estimation error of a SSKF without and with the proposed residual harmonics state, in (a) and (b), respectively.

III. Compensating OPPs for Voltage Harmonics

Equipped with a means to estimate grid voltage harmonics, we now explore a method that has the potential to improve the harmonic performance of OPPs. The objective is to compensate an OPP for voltage harmonics that may emerge at converter's PCC, such as when the grid voltage is distorted.

A pulse pattern is formulated from Fourier Coefficients. These are a function of up to k switching angles, α, which vary slightly depending on the waveform's odd symmetry and number of output levels. For example, the Fourier Coefficients of a three-level (3L) pulse pattern with quarter-wave (QW) or half-wave (HW) symmetry can be parameterized as:

$$\begin{aligned} a_n &= \rho_a \cdot \sum_{i=1}^{\mathcal{K}} (-1)^i \cdot \sin(n\alpha_i) \\ b_n &= \rho_b \cdot \sum_{i=1}^{\mathcal{K}} (-1)^i \cdot \cos(n\alpha_i) \end{aligned} \tag{10}$$

$$\mathcal{K} = \begin{cases} k \\ 2k \end{cases} \qquad \rho_a = \begin{cases} 0 \\ \frac{-2}{n\pi} \end{cases} \qquad \rho_b = \begin{cases} \frac{4}{n\pi} & \text{QW} \\ \frac{2}{n\pi} & \text{HW} \end{cases}$$

Where the effective switching frequency is $f_{sw} = k \cdot f_1$ Hz.

Assuming a 3L-HW pulse pattern with five switching angles in the first quarter-cycle, the Fourier Coefficients are then:

$$\begin{aligned} a_n &= \frac{-2}{n\pi} \cdot \sum_{i=1}^{10} (-1)^i \cdot \sin(n\alpha_i) \\ b_n &= \frac{2}{n\pi} \cdot \sum_{i=1}^{10} (-1)^i \cdot \cos(n\alpha_i) \end{aligned} \tag{11}$$

Quarter-wave (QW) symmetry is deliberately not assumed. By eliminating a_n, the phase of a pulse pattern's harmonics are then constrained to $0°$ or $180°$. Consequently, QW pulse patterns cannot be compensated for grid voltage harmonics since the phase of distortions in the grid are diverse.

A. Grid Voltage Fourier Coefficients

To incorporate the estimated grid voltage harmonics, $\hat{\boldsymbol{v}}_{g,\alpha\beta;h}$, into the objective function of a pulse pattern, they must be transformed from a vector in $\alpha\beta$ into two scalars; their Fourier Coefficients, $\boldsymbol{v}_{g,F;h} = [\boldsymbol{v}_{g,F;1}, \boldsymbol{v}_{g,F;5}, \cdots, \boldsymbol{v}_{g,F;N},]^T$.

Firstly, we apply a modified Park Transformation to each harmonic:

$$\boldsymbol{v}_{g,F;n} = \begin{bmatrix} v_{g,a;n} \\ v_{g,b;n} \end{bmatrix} = \begin{bmatrix} 1 & 0 \\ 0 & -1 \end{bmatrix} \cdot \boldsymbol{T}_{\alpha\beta-dq} \cdot \boldsymbol{v}_{g,\alpha\beta;n} \quad (12)$$

where,

$$\begin{aligned} \boldsymbol{T}_{\alpha\beta-dq} &= \begin{bmatrix} \cos(\theta_n + \Delta\phi_n) & \sin(\theta_n + \Delta\phi_n) \\ -\sin(\theta_n + \Delta\phi_n) & \cos(\theta_n + \Delta\phi_n) \end{bmatrix} \\ \theta_n &= \tan^{-1}\left(v_{g,\beta;n}/v_{\alpha;n}\right) \\ \Delta\phi_n &= n\theta_1 - \theta_n \end{aligned} \quad (13)$$

The fundamental's phase is shifted by $n\theta_1$, so it is in synchronism with the harmonic's phase θ_n. Similar to a PLL, since their frequency is equal their phase displacement, $\Delta\phi_n$, is constant. Then, recalling the polar representation of Fourier Coefficients, $\vec{V}_n = a_n - jb_n$, the positive- and negative-sequence quadrature components are inverted to align them with b_n.

Secondly, their phase is adjusted to negate the phase shift introduced by a grid-connected converter:

$$\vec{U}^*_{i;1} = \vec{I}^*_{g;1} \cdot \vec{Z}_{eq;1} + \vec{V}_{g;1} \quad (14)$$

where,

$$\begin{aligned} \vec{U}^*_{i;1} &= U^*_{i;1}\angle\phi^*_u & \vec{I}^*_{g;1} &= I^*_{g;1}\angle\phi^*_1 \\ \vec{Z}_{eq;1} &= R_{eq} + j\omega_1 L_{eq} & \vec{V}_{g;1} &= v_{g,b;1}\angle\phi_{g;1} \end{aligned} \quad (15)$$

To align with the pulse pattern's odd symmetry (11), the grid voltage is assumed to have no cosine component, so $v_{g,a;1} = 0$, and $\phi_{g;1} = \arg(-jv_{g,b;1}) = -90°$. In our case, the equivalent grid impedance, $\vec{Z}_{eq;1}$, is a lumped RL component. For the fundamental grid current setpoint, $\vec{I}^*_{g;1}$, a unity power factor is assumed, so $\phi^*_1 = \phi_{g;1}$.

To then yield the Fourier Coefficients for the remaining, $n > 1$, grid voltage harmonics, we attenuate the DC-link voltage and adjust their phase by $n\phi^*_u$,

$$\begin{aligned} \vec{U}_{g;n} &= \frac{2}{V_{DC}}\left(v_{g;a;n} - jv_{g;b;n}\right)e^{-jn\phi^*_u} \\ &= u_{g;a;n} + ju_{g;b;n} \end{aligned} \quad (16)$$

In summary, using (12) - (16), the estimated grid voltage harmonics, $\hat{\boldsymbol{v}}_{g,\alpha\beta;h}$, can be transformed into their Fourier Coefficients, $\vec{U}_{g;n}$. Now, they are compatible with the objective function of a pulse pattern and can thus be compensated for. A key step is adjusting the grid voltage harmonic's phase so the phase shift introduced by the converter, ϕ^*_u, is negated.

B. Objective Function

The nonlinear constrained (NLC) objective function for a 3L-HW OPP with an RL output filter that compensates for voltage harmonics whilst constrained to grid code limits is:

$$\begin{aligned} \min_{\boldsymbol{\alpha}} \quad & f(\boldsymbol{\alpha}) = \sum_{n=5,7,11,\ldots}^{\geq 50} \frac{\Delta a_n^2 + \Delta b_n^2}{n^2} \\ \text{subject to} \quad & a_1 = 0,\ b_1 = m^* \\ & \alpha_1 \leq \alpha_2 \leq \ldots \leq \alpha_{2k} \leq \pi \\ & \left|\vec{I}_{g;n}/\vec{I}^*_{g;1}\right| \leq I^{LIM}_{g;n} \end{aligned} \quad (17)$$

Where,

$$\begin{aligned} \Delta a_n &= u_{i,a;n} - u_{g,a;n} & \Delta b_n &= u_{i,b;n} - u_{g,b;n} \\ \vec{I}_{g;n} &= \Delta\vec{V}_{i;n} \cdot \vec{Z}_{eq;n} & \Delta\vec{V}_{i;n} &= \frac{V_{DC}}{2}(\Delta a_n - j\Delta b_n) \end{aligned} \quad (18)$$

Note that $u_{i,a;n} = a_n$ and $u_{i,b;n} = b_n$ are the Fourier Coefficients of the pulse pattern from (11), so they are functions of the optimization variable, $\boldsymbol{\alpha} = [\alpha_1, \cdots, \alpha_{2k}]^T$. The difference between them and the grid voltage Fourier Coefficients are encapsulated by Δa_n and Δb_n. Any mismatch between harmonics is penalised by the familiar $1/n^2$ weighting since $\vec{Z}_{eq;n}$ is an RL impedance. The grid current, $\vec{I}_{g;n}$, is yielded by the voltage, $\Delta\vec{V}_{i;n}$, impressed across $\vec{Z}_{eq;n}$, for each harmonic.

Regarding the equality constraints, the fundamental is strictly a sine wave, so $a_1 = 0$. The setpoint modulation index is yielded from (14) by attenuating the DC-link voltage of a 3L converter, $b_1 = U^*_{i;1} \cdot 2/V_{DC} = m^* \in [0, 4/\pi]$.

Regarding the inequality constraints, the switching angles are ascending and confined to the positive half-cycle. Conformance to grid code limits is imposed by the $I^{LIM}_{g;n}$ constraint if $\vec{I}^*_{g;1} > 0$. This ensures the per-unit magnitude of each grid current harmonic, $\left|\vec{I}_{g;n}/\vec{I}^*_{g;1}\right|$, is below the limit set by $I^{LIM}_{g;n}$.

C. Numerical Results

To explore the potential improvements of compensating pulse patterns for voltage harmonics, SHE and OPPs assuming an ideal grid voltage are compared against their proposed grid-voltage-compensated counterparts. Numerical results for a MV converter case study are shown in Fig. 3. The system model used is derived from [11] and is given below in Table I.

TABLE I: SYSTEM MODEL PARAMETERS

Parameter	Symbol	SI Value	pu
Rated Apparent Power	S_B	9 MVA	1.0
Rated Voltage	V_B	3.15 kV	1.0
Rated Current	I_B	1.65 kA	1.0
Rated Frequency	f_1	50 Hz	1.0
DC-Link Voltage	V_{DC}	4.84 kV	1.53
Filter ESL	L_f	876 μH	0.25
Filter ESR	R_f	16.8 mΩ	0.018
Grid ESL	L_g	351 μH	0.1
Grid ESR	R_g	11 mΩ	0.025
Grid Voltage	V_g	3.15 kV	1.0

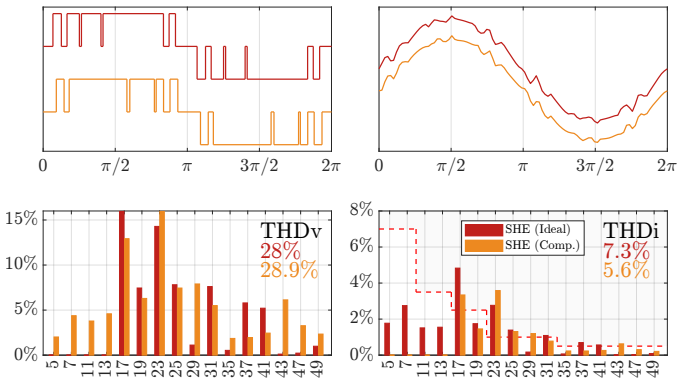

(a)

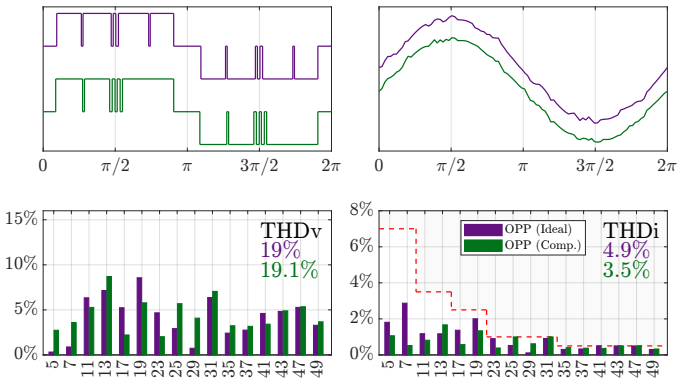

(b)

Fig. 3: Numerical results of two cases for SHE and OPPs, shown above in (a) and (b), respectively. The first case assumes an ideal grid voltage, as today's methods do. The second case compensates the pulse pattern for grid voltage harmonics, as proposed in this paper by (17). The red dotted line shown in the FFT of the grid current is the IEEE-519 grid code harmonic limits for $20 < I_{SC}/I_L < 50$.

For all results, the grid voltage is distorted with the 5^{th}-13^{th} NTO harmonics as shown earlier in Fig 2. In per-unit, they are, $\vec{V}_{g;5} = 0.0211\angle 236°$, $\vec{V}_{g;7} = 0.0458\angle 12°$, $\vec{V}_{g;11} = 0.0396\angle 305°$ and $\vec{V}_{g;5} = 0.0480\angle 336^o$. Whereas $|\vec{I}^*_{g;1}| = 1.0$pu, so m^* = 1.12 as yielded from (14).

Examining SHE, the proposed grid-voltage-compensated alternative rejects the 5^{th}-13^{th} grid voltage harmonics, as shown by the non-zero orange bars in the magnitude spectrum of the pulse pattern; bottom left plot of Fig. 3a. In doing so, the respective current harmonics are correctly eliminated. This is in contrast to SHE when assuming an ideal grid voltage. By design, it has eliminated the 5^{th}-13^{th} voltage harmonics of the pulse pattern. Consequently, the converter's current is freely corrupted by the grid voltage distortions, as shown by the corresponding non-zero red bars in the magnitude spectrum of the grid current; bottom right plot of Fig. 3a.

Whereas for the OPP shown in Fig. 3b, by compensating it for the grid voltage harmonics using (17), it is able to exploit the grid voltage harmonics to reduce THDi from 4.9% to 3.5%; an improvement of almost 30%. In addition, it is worth highlighting the superior harmonic performance of OPPs when compared to SHE. By considering more harmonics within its objective function and weighting them by the frequency response of the converter's equivalent output impedance, a broader spectrum of current harmonics can then be minimized.

These numerical results validate the potential to improve an OPP's harmonic performance by compensating it for grid voltage harmonics at a converter's PCC. The outstanding challenge, as detailed within the succeeding section, is implementing an algorithm to perform all of this in real-time.

IV. Implementing a Real-time OPP Solver

To compensate an OPP for the estimated grid voltage harmonics in real-time, an algorithm is proposed to interface a NLC solver with the SSKF. The objective is to determine when and if a new OPP should be computed or applied by the converter. A hardware architecture capable of executing fixed sample rate algorithms in conjunction with a powerful solver for NLC optimization is proposed. Then, a real-time OPP solving algorithm is distilled into a flow chart.

A key assumption that enables the real-time computation of an OPP from (17) is the rate at which grid voltage harmonics vary. In this paper, we assume they change slowly with respect to the fundamental frequency. In other words, over a few seconds. This assumption is fair when considering that harmonic performance, such as THD, is measured in the steady-state. Therefore, by acknowledging that optimizing harmonic performance is not a time-critical task, this may afford sufficient time to compute an OPP in real-time.

During transient events, harmonic performance is not a priority and a pulse pattern controller [28]–[30] would intervene. One proposal the authors intend to explore is leveraging a LUT as a fallback during transients. To explain, the real-time OPP yielded from (17) is regulated in the steady-state. Whereas during transients, the pulse pattern controller can fallback to a LUT since larger adjustments may be needed. Upon returning to the steady-state, it can transition back to regulating the real-time OPP to yield improved harmonic performance.

A. Hardware Architecture

The proposed hardware architecture consists of two platforms that communicate over a full-duplex serial bus, as shown in Fig. 4. One is an MCU to perform time-critical tasks, such as implementing a SSKF and a pulse pattern modulator. The other, is an MPU that performs more computationally intensive tasks, such as NLC optimization for the real-time OPP solver.

Given grid voltage measurements, $\boldsymbol{v}_{g,abc}$, the SSKF estimates the harmonics, $\hat{\boldsymbol{v}}_{g,\alpha\beta;h}$. These are passed to a steady-state detector. The purpose of this stage is to determine when the grid voltage harmonics are in the steady-state, as only then is a real-time OPP needed. It is implemented as a comparison of past and present grid voltage harmonic coefficients against a user-defined threshold, $|\hat{\boldsymbol{v}}_{g,F;h}(k-1) - \hat{\boldsymbol{v}}_{g,F;h}(k)| < \rho_{SS}$.

If the above expression returns true for all harmonics, the estimated steady-state grid voltage Fourier Coefficients, $\hat{\boldsymbol{V}}_{g,F;h}$, are transmitted to the MPU. Here, a multi-threaded Sequential

Quadratic Programming (SQP) solver is implemented to parallelize and expedite the real-time OPP solver. All cores share a queue of initial points from a Halton Sequence and update a shared optimal solution, α_{2k}^{opt}, when a better OPP is found. This is then transmitted back to the MCU so a modulator can generate the pulse pattern.

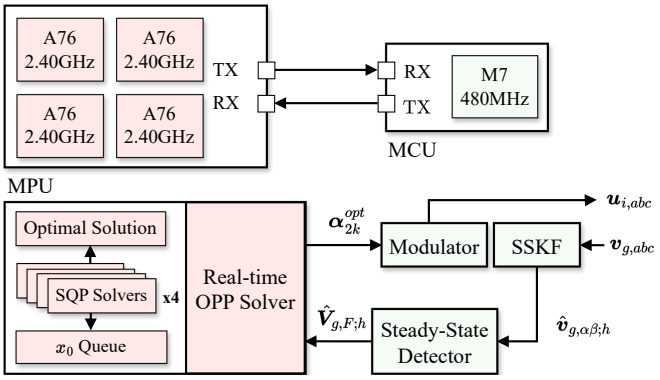

Fig. 4: Proposed hardware architecture to implement an algorithm for computing OPPs in real-time to compensate for estimated grid voltage harmonics.

B. Algorithm Flowchart

An algorithm for computing OPPs in real-time is illustrated as a flow chart in Fig. 5. The key step in this algorithm is updating the optimal solution, f_{opt}, to the applied OPP in respect to the new grid voltage harmonics, $\boldsymbol{u}_{g,F;h}$. This ensures the harmonic performance of the OPP applied by the converter can only be improved, as this is the benchmark for awarding a better OPP when $f_{cand} < f_{opt}$.

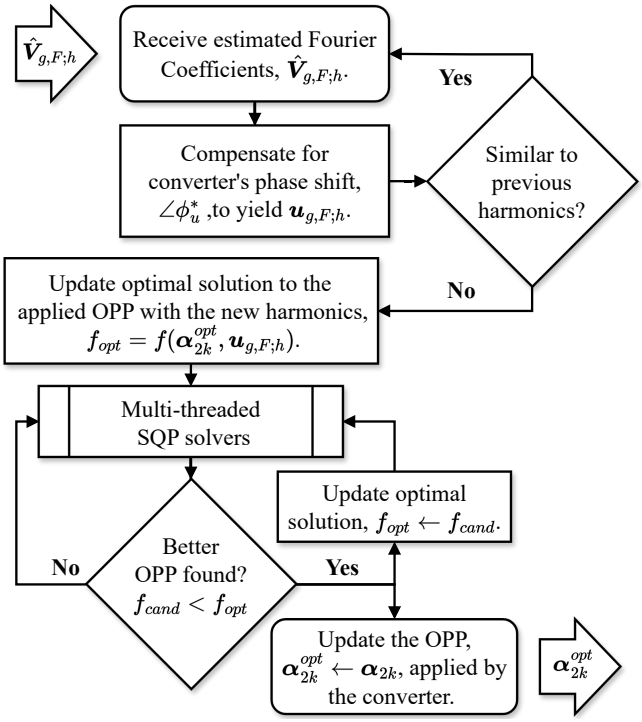

Fig. 5: Flowchart of the proposed real-time OPP solver.

V. Experimental Results

A Hardware-In-The-Loop (HIL) approach is used to acquire experimental result, as shown by the setup in Fig. 6. The converter and system model given in Table I is implemented in the OPAL-RT, whereas the real-time OPP solver and SSKF are implemented in C++ code on the MPU and MCU, respectively.

Since distortions in the grid voltage are generally unknown, a true random number generator on a separate core of the MCU is used to generate a distorted grid voltage, $\boldsymbol{v}_{g,abc}$. This and the OPP, $\boldsymbol{u}_{i,abc}$, are the two inputs to the OPAL-RT that is modelling the grid-connected converter system. To estimate the grid voltage harmonics in real-time, it is passed through the OPAL-RT to an analog output and sampled at a rate of 5kHz by the main core of the MCU that executes the SSKF.

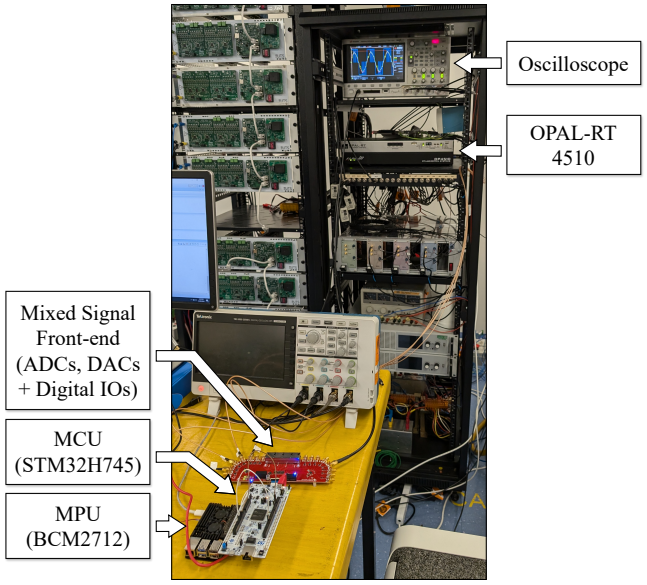

Fig. 6: Laboratory setup for experimental results.

The primary challenge in computing OPPs for compensation of estimated grid voltage harmonics is doing so in real-time. Therefore, the focus is on the time taken for the real-time OPP solver to yield improvements in harmonic performance.

A. Real-time OPP Solver Computation Times & Improvements

The protocol is applying a step from an ideal to a randomly distorted grid voltage for two cases. One case limits the randomized magnitude of the 5^{th}-13^{th} NTO grid voltage harmonics to 5% of the fundamental, whereas the second case raises the limit to 10%. For both cases, there is no limit on the grid voltage harmonic's randomized phase.

A single run of this protocol is shown as consecutive snapshots in time by Fig. 7a - 7c. At t=0ms, the grid voltage is stepped from ideal to distorted; notice the immediate affect these voltage harmonics have on the converter's grid current. So much so, the 5^{th} harmonic now voids the IEEE-519 current distortion limit for $50 < I_{sc}/I_L < 100$. As shown by the pink bar surpassing the red dotted line in the magnitude spectrum of the converter's grid current in Fig. 7a.

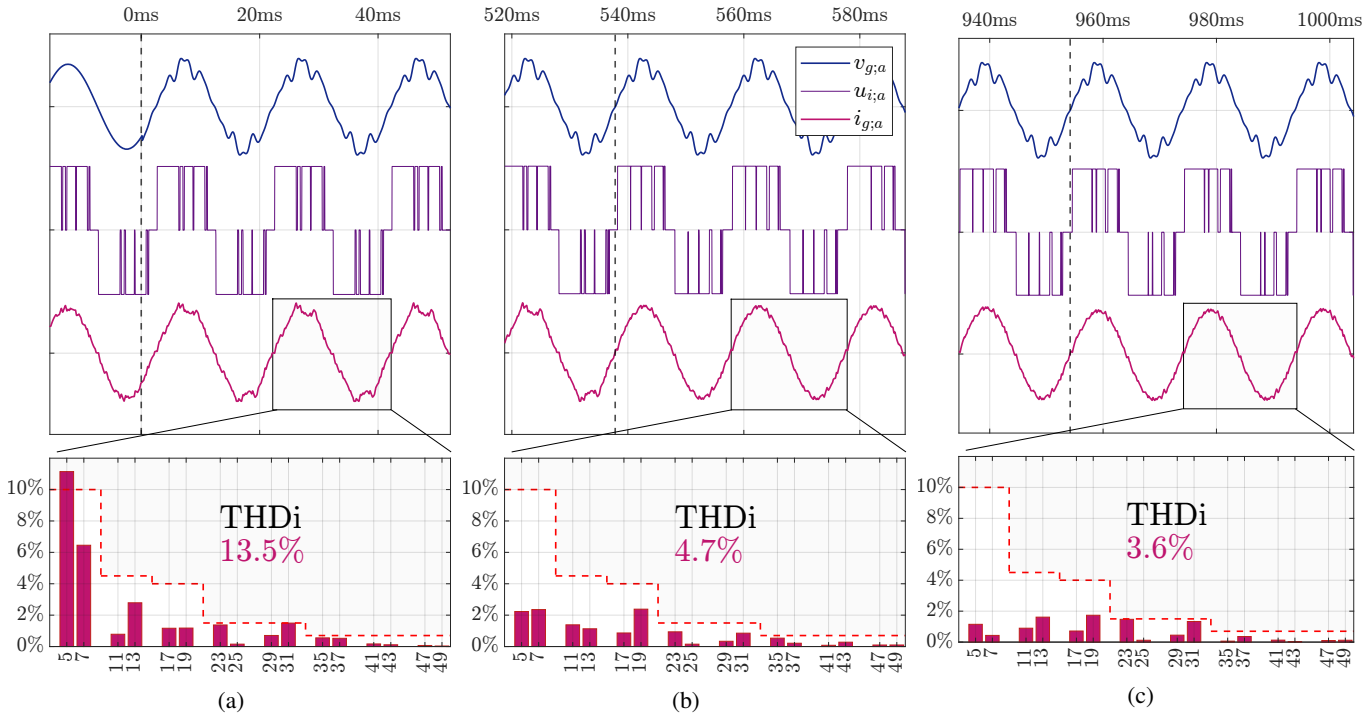

Fig. 7: Experimental results of the real-time OPP solver reducing distortions in the converter's grid current upon a step change from an ideal to a distorted grid voltage at t=0ms. The 5^{th}-13^{th} grid voltage harmonics are randomized and limited to 10% of the fundamental's magnitude. Black dotted lines in (b) and (c) indicate when a better OPP has been computed and is applied.

The initial THDi of 13.5% is the benchmark for improvements in harmonic performance yielded by the real-time OPP solver. Comparisons to an ideal grid voltage are irrelevant since the THDi shown in Fig. 7a is the performance of an incumbent OPP; one that assumes an ideal grid voltage. Shortly after this step, the algorithm depicted in Fig. 5 commences when the real-time OPP solver receives the estimated Fourier Coefficients of the grid voltage, $\hat{\boldsymbol{V}}_{g,F;h}$ from the SSKF.

Focusing on Fig. 7b, at t=540ms the real-time OPP solver returns the first OPP that is compensated for the distorted grid voltage. Upon the converter applying it, THDi is reduced from 13.5% to 4.7%; an improvement of more than 60%.

Then, an even better OPP is found after 410ms and is applied at t =960ms, as shown in Fig. 7c. The improvement in harmonic performance yielded by the real-time OPP solver then exceeds 70%. Recall that this improvement is in respect to the OPP assuming an ideal grid voltage from Fig. 7a.

To more thoroughly explore the real-time OPP solver, the above protocol is repeated 600 times for randomly distorted grid voltages, as per the two cases mentioned earlier in this section. The runtime is extended to 10s to examine when the real-time OPP solver begins to converge to a global minimum.

Examining Fig. 8a, the median reduction in THDi is more than 25% after 600ms. Beyond this, the improvements climb to 35% by 3s and then flat line at 40%. Whereas for Fig. 8b, there is a similar trend of diminishing improvements beyond 600ms and by 3s they settle within 5% of their final value.

A promising observation is the median reduction in THDi being significantly higher with a more distorted grid voltage.

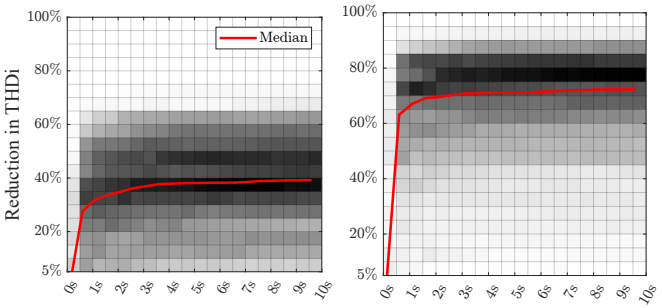

Fig. 8: 2D histograms (n=600) depicting the real-time OPP solver reducing the THDi of the converter's grid current upon applying a step change from an ideal to a randomly distorted grid voltage. In (a), the 5^{th}-13^{th} NTO grid voltage harmonics are randomized and limited to 5% of the fundamental's magnitude. Whereas in (b), this limit is raised to 10% to explore a more distorted grid voltage. Darker colours indicate a higher density of data and the median reduction in THDi as the real-time OPP solver executes is shown by a red line.

This is shown by Fig. 8b, where the real-time OPP solver's median improvement in harmonic performance exceeds 70%. This suggests that the proposed grid-voltage-compensated OPPs have the potential to outperform incumbent OPP's as distortions at the converter's PCC voltage continue to increase.

In summary, the experimental results support that it is feasible to compensate OPPs for a distorted PCC voltage in real-time, assuming distortions vary every few seconds.

VI. Conclusion

In this paper, we have explored compensating OPPs for the effect of voltage harmonics in the context of a grid-connected converter with a distorted PCC voltage; a challenging scenario that is encountered in practice. Addressing this research gap has shown that OPPs can be computed in real-time without the use of LUTs or complex data structures, as verified by thorough experimental results using commercial hardware.

The closing remark is that the proposed grid-voltage-compensated OPPs have the potential to significantly improve harmonic performance in comparison to incumbent OPPs that assume an ideal grid voltage. A promising observation is the headroom for improvement is correlated to the magnitude of harmonics in the grid voltage - so the proposed approach can excel where incumbent OPPs are most deficient.

Future work is exploring weak grid scenarios and interfacing real-time OPPs with a pulse pattern controller to leverage the improved harmonic performance in the steady-state.

Acknowledgment

This paper is supported by the University of Technology Sydney in collaboration with ABB Motion System Drives.

References

[1] H. S. Patel and R. G. Hoft, "Generalized Techniques of Harmonic Elimination and Voltage Control in Thyristor Inverters: Part I–Harmonic Elimination," *IEEE Transactions on Industry Applications*, vol. IA-9, no. 3, pp. 310–317, May 1973.

[2] M. S. A. Dahidah, G. Konstantinou, and V. G. Agelidis, "A review of multilevel selective harmonic elimination pwm: Formulations, solving algorithms, implementation and applications," *IEEE Transactions on Power Electronics*, vol. 30, no. 8, pp. 4091–4106, 2015.

[3] L. G. Franquelo, J. Napoles, R. C. P. Guisado, J. I. Leon, and M. A. Aguirre, "A flexible selective harmonic mitigation technique to meet grid codes in three-level PWM converters," *IEEE Transactions on Industrial Electronics*, vol. 54, no. 6, pp. 3022–3029, Dec. 2007.

[4] J. Napoles, J. I. Leon, R. Portillo, L. G. Franquelo, and M. A. Aguirre, "Selective harmonic mitigation technique for high-power converters," *IEEE Transactions on Industrial Electronics*, vol. 57, no. 7, pp. 2315–2323, Jul. 2010.

[5] T. Geyer, *Model Predictive Control of High Power Converters and Industrial Drives*. Wiley, 2017.

[6] P. Karamanakos, M. A. Waris Begh, S. Rahmanpour, and T. Geyer, "Gradient-based predictive pulse pattern control for grid-connected converters with lcl filters," in *2023 IEEE Energy Conversion Congress and Exposition (ECCE)*, 2023, pp. 2645–2652.

[7] T. Dorfling, H. d. T. Mouton, and T. Geyer, "Generalized model predictive pulse pattern control based on small-signal modeling—part 2: Implementation and analysis," *IEEE Transactions on Power Electronics*, vol. 37, no. 9, pp. 10 488–10 498, 2022.

[8] V. Spudić and T. Geyer, "Fast control of a modular multilevel converter statcom using optimized pulse patterns," in *2017 IEEE Energy Conversion Congress and Exposition (ECCE)*, 2017, pp. 2707–2714.

[9] R. Teodorescu, M. Liserre, and P. Rodríguez, *Grid Converters for Photovoltaic and Wind Power Systems*. Wiley, Dec. 2010.

[10] S. Elphick, P. Ciufo, G. Drury, V. Smith, S. Perera, and V. Gosbell, "Large scale proactive power-quality monitoring: An example from australia," *IEEE Transactions on Power Delivery*, vol. 32, no. 2, pp. 881–889, Apr. 2017.

[11] J. David, S. Elphick, and D. Robinson, "Management of harmonic distortion for large renewable energy generation," in *2022 32nd Australasian Universities Power Engineering Conference (AUPEC)*. IEEE, Sep. 2022.

[12] S. Elphick, V. Gosbell, V. Smith, S. Perera, P. Ciufo, and G. Drury, "Methods for harmonic analysis and reporting in future grid applications," *IEEE Transactions on Power Delivery*, vol. 32, no. 2, pp. 989–995, Apr. 2017.

[13] G. S. Buja, "Optimum output waveforms in PWM inverters," *IEEE Transactions on Industry Applications*, vol. IA-16, no. 6, pp. 830–836, Nov. 1980.

[14] A. Birth, T. Geyer, H. d. T. Mouton, and M. Dorfling, "Generalized three-level optimal pulse patterns with lower harmonic distortion," *IEEE Transactions on Power Electronics*, vol. 35, no. 6, pp. 5741–5752, 2020.

[15] S. Rahmanpour, P. Karamanakos, and T. Geyer, "Three-level optimized pulse patterns for grid-connected converters with LCL filters," in *2023 IEEE Energy Conversion Congress and Exposition (ECCE)*, 2023, pp. 1430–1437.

[16] J. David, D. Robinson, and S. Elphick, "Aggregation of multiple inverter-based harmonic sources within a renewable energy generation plant," in *2022 20th International Conference on Harmonics &; Quality of Power (ICHQP)*. IEEE, May 2022.

[17] A. D. Birda, J. Reuss, and C. Hackl, "Synchronous optimal pulse-width modulation with differently modulated waveform symmetry properties for feeding synchronous motor with high magnetic anisotropy," in *2017 19th European Conference on Power Electronics and Applications (EPE'17 ECCE Europe)*, 2017, pp. P.1–P.10.

[18] G. Darivianakis and I. Tsoumas, "Insight into the peculiarities of optimized pulse patterns for permanent-magnet synchronous machines," in *2020 22nd European Conference on Power Electronics and Applications (EPE'20 ECCE Europe)*, 2020, pp. P.1–P.8.

[19] E. Kontodinas, P. Karamanakos, A. Kraemer, and S. Wendel, "Optimized pulse patterns for synchronous machines with non-sinusoidal back-emf," in *2023 25th European Conference on Power Electronics and Applications (EPE'23 ECCE Europe)*, 2023, pp. 1–9.

[20] I. Ibanez-Hidalgo, A. Sanchez-Ruiz, A. Perez-Basante, A. Zubizarreta, S. Ceballos, S. Gil-Lopez, and R. P. Aguilera, "Real time selective harmonic control—PWM based on ANNs," *IEEE Transactions on Power Electronics*, vol. 39, no. 1, pp. 768–783, Jan. 2024.

[21] F. Huerta, J. Perez, S. Cobreces, and M. Rizo, "Frequency-adaptive multiresonant LQG state-feedback current controller for LCL-filtered VSCs under distorted grid voltages," *IEEE Transactions on Industrial Electronics*, vol. 65, no. 11, pp. 8433–8444, nov 2018.

[22] R. Cardoso, R. F. de Camargo, H. Pinheiro, and H. A. Gründling, "Kalman filter based synchronization methods," in *2006 37th IEEE Power Electronics Specialists Conference*. IEEE, Jun. 2006.

[23] J. M. Kanieski, R. Cardoso, H. Pinheiro, and H. A. Grundling, "Kalman filter-based control system for power quality conditioning devices," *IEEE Transactions on Industrial Electronics*, vol. 60, no. 11, pp. 5214–5227, Nov. 2013.

[24] K. Kennedy, G. Lightbody, and R. Yacamini, "Power system harmonic analysis using the kalman filter," in *2003 IEEE Power Engineering Society General Meeting (IEEE Cat. No.03CH37491)*, vol. 2, 2003, pp. 752–757 Vol. 2.

[25] C. Fischer, S. Mariéthoz, and M. Morari, "A model predictive control approach to reducing low order harmonics in grid inverters with LCL filters," in *IECON 2013 - 39th Annual Conference of the IEEE Industrial Electronics Society*, 2013, pp. 3252–3257.

[26] S. Vazquez, E. Zafra, R. P. Aguilera, T. Geyer, J. I. Leon, and L. G. Franquelo, "Prediction model with harmonic load current components for fcs-mpc of an uninterruptible power supply," *IEEE Transactions on Power Electronics*, vol. 37, no. 1, pp. 322–331, 2022.

[27] K. J. Åström and B. Wittenmark, *Computer-controlled systems (3rd ed.)*. USA: Prentice-Hall, Inc., 1997.

[28] T. Geyer, N. Oikonomou, G. Papafotiou, and F. D. Kieferndorf, "Model predictive pulse pattern control," *IEEE Transactions on Industry Applications*, vol. 48, no. 2, pp. 663–676, 2012.

[29] R. P. Aguilera, P. Acuña, P. Lezana, G. Konstantinou, B. Wu, S. Bernet, and V. G. Agelidis, "Selective harmonic elimination model predictive control for multilevel power converters," *IEEE Transactions on Power Electronics*, vol. 32, no. 3, pp. 2416–2426, 2017.

[30] L. Rosado, J. Samanes, E. Gubia, and J. Lopez, "Selective harmonic mitigation: Limitations of classical control strategies and benefits of model predictive control," *IEEE Transactions on Industry Applications*, vol. 59, no. 5, pp. 6082–6094, Sep. 2023.

[31] G. C. Goodwin, S. F. Graebe, and M. E. Salgado, *Control system design*. Pearson India Education, 2016.

[32] F. Huerta, D. Pizarro, S. Cobreces, F. J. Rodriguez, C. Giron, and A. Rodriguez, "Lqg servo controller for the current control of LCL grid-connected voltage-source converters," *IEEE Transactions on Industrial Electronics*, vol. 59, no. 11, pp. 4272–4284, nov 2012.